Earthquakes and Structures, *Vol. 15, No. 1 (2018) 97-111*
DOI: https://doi.org/10.12989/eas.2018.15.1.097

A simplified design approach for modelling shear force demand on tower walls supported on a transfer structure in regions of lower seismicity

Mehair Yacoubian[*1], Nelson Lam[1a], Elisa Lumantarna[1b] and John L. Wilson[2a]

[1]*Department of Infrastructure Engineering, The University of Melbourne, Parkville, Victoria 3010, Australia*
[2]*Centre for Sustainable Infrastructure, Swinburne University of Technology, Hawthorn, Victoria 3122, Australia*

(Received February 20, 2018, Revised May 25, 2018, Accepted May 28, 2018)

Abstract. Buildings featuring a transfer structure can be commonly found in metropolitan cities situated in regions of lower seismicity. A transfer structure can be in the form of a rigid plate or an array of deep girders positioned at the podium level of the building to support the tower structure of the building. The anomalous increase in the shear force demand on the tower walls above the podium is a major cause for concern. Design guidance on how to quantify these adverse effects is not available. In this paper a simplified method for quantifying the increase in the shear force demand on the tower walls is presented. In view of the very limited ductile nature of this type of construction the analysis presented herein is based on linear elastic behaviour.

Keywords: displacement-controlled behaviour; transfer structures; transfer plate; transfer girder; tower walls

1. Introduction

Buildings incorporating the use of a transfer plate, or transfer girders, as a structural feature at the podium level of the building can be commonly found in metropolitan cities in regions of lower seismicity. A transfer structure has the function of redistributing gravitational loads where there is a discontinuity in the load path to accommodate a major change in the architectural layout of floor spaces in the building. It can be regarded as a major feature of vertical irregularity which is expected to compromise the ductility of the building in projected seismic conditions (ASCE 2010, CEN 2005). Even then many such buildings have been designed and built in regions of lower seismicity.

Research has been undertaken to investigate the potential seismic performance of buildings featuring the use of a transfer structure at the podium level by the use of shaking table testing of scaled down models (Li *et al*. 2006, Lee and Hwang 2015). Analytical investigations have also been undertaken to reveal a significant increase in the ductility demand of the building as a result of this type of vertical irregularity (Mwafy and Khalifa 2017). Studies have also gained insights into the potential adverse effects of the flexural stiffness of the transfer structure on the seismic behaviour of the building both locally (in the vicinity of the location of the transfer structure) and globally on the building as a whole (Su *et al*. 2002, 2008, 2009, Zhitao 2000, Qian and Wang 2006). A significant anomalous increase in the shear force on the tower wall above the transfer floor level (TFL) has been confirmed by experimental investigations as reported in Li *et al*. (2005, 2008) and Kuang and Zhang (2003).

In a literature review publication by Su *et al*. (2011) the phenomenon of displacement controlled behaviour which puts the “cap” on the displacement demand behaviour of a flexible structure was introduced. An analysis methodology which incorporates considerations of the displacement demand behaviour of the building in comparison with its displacement capacity (Priestley *et al*. 2007, Priestley 1997, Tsang *et al*. 2009) would result in robust predictions of the seismic performance behaviour of the building which has incorporated the use of a transfer structure.

The next section presents examples of the anomalous increase in the shear force demands on the tower walls which are supported by a transfer structure. The shear force increase is particularly pronounced above the podium level where the transfer structure is positioned. In subsequent sections of the paper a simplified method will be developed to quantify the adverse effects. In the final section of the chapter the introduced method of prediction is illustrated by the use of a worked example.

2. Shear force anomalies in tower walls above the TFL

Earlier investigations on buildings featuring a transfer plate have highlighted the onset of high shear concentrations occurring in the tower walls above the transfer floor level (TFL) as the building is subjected to lateral loads (Su *et al.* 2002, Tang and Su 2014). These shear stress concentrations can be resulted mainly from out-of-plane bending of the transfer structure supporting the tower walls. Differential rotation of the transfer structure along its length results in displacement incompatibility in between adjacent tower walls. The incompatibility induces high in-plane forces in elements (link beams and slabs)

∗Corresponding author, Ph.D. Candidate
E-mail: myacoubian@student.unimelb.edu.au
[a]Professor
[b]Lecturer

http://www.techno-press.com/journals/eas&subpage=7

ISSN: 2092-7614 (Print), 2092-7622 (Online)

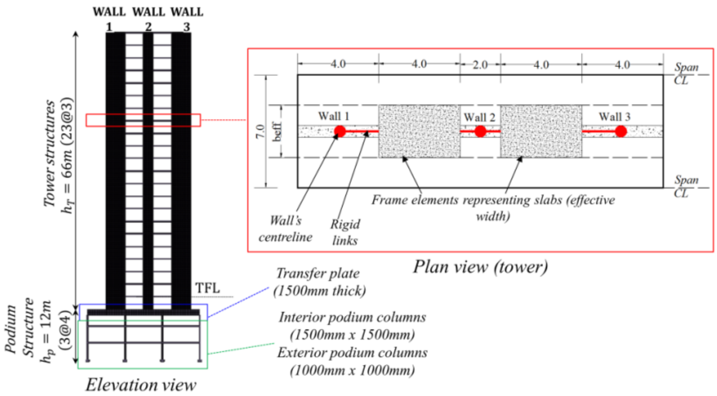

Fig. 1 2D model of the building featuring a transfer plate

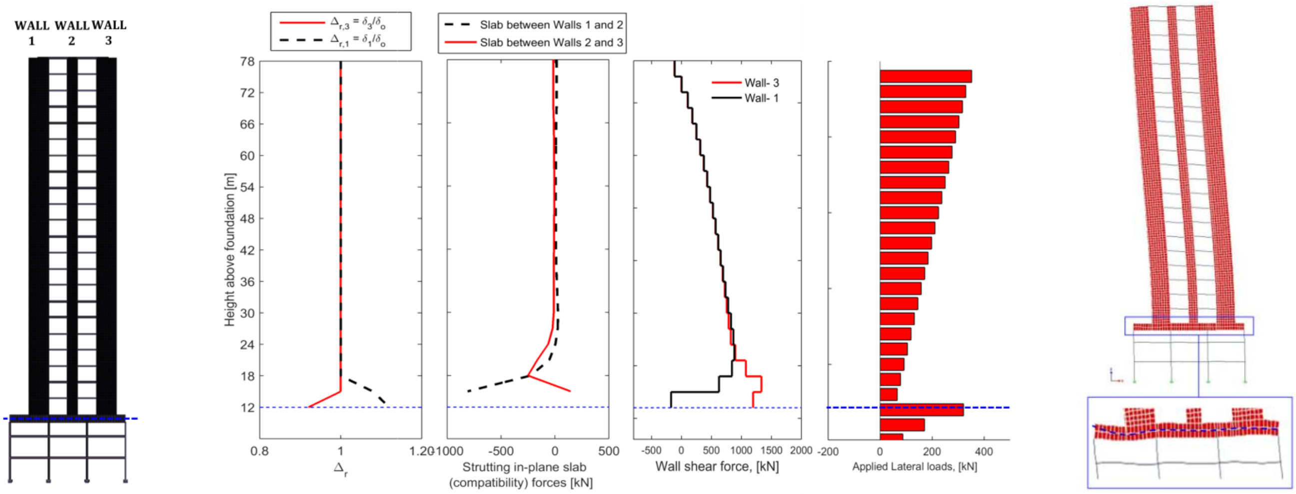

(a) 2D planar model of the building

(b) Displacement ratio

(c) Strutting forces in the connecting slabs

(d) Shear force distribution in the tower walls

(e) Applied lateral load profile

(f) Out-of-plane bending of the transfer plate

Fig. 2 Displacement incompatibility between connected walls and the resulting strutting (compatibility) slab force and wall shear force distributions

connecting the tower walls thereby resulting in a significant increase in the shear force above the TFL. Similar shear force distribution anomalies have been reported for tower walls featuring setbacks (Yacoubian *et al*. 2017a).

The 2D model of an example building (Fig. 1) was employed to illustrate such shear force anomalies. The numerical FE model (of the building) is constructed on program ETABS where 2D shell elements have been used for the modelling of the tower walls and the transfer plate. Elastic frame elements have been employed for the modelling of the stiff podium column and the floor slabs represented by their effective widths (refer to Yacoubian *et al*. 2017b for more details). There are three tower walls in the considered example building. Each of the tower walls is assigned a number (1-3). The exterior walls are no. 1 and 3 whereas the wall in the middle is no. 2 (refer Fig. 2(a)). The displacement ratio (Δ_r) is introduced herein as the ratio of the lateral displacement of wall no. 1 (δ_1), or wall no. 3 (δ_3), divided by the respective displacement (δ_o) of a control model wherein the transfer plate was modelled as infinitely rigid when bending out-of-plane. The building models (control and actual) have been subjected to the same lateral loads with magnitudes given in Fig. 2(e). In the control model all three walls have identical deflection profile. The increase in the shear force demand on wall no. 3 (which is paralleled by a reduction in the shear force demand on wall no. 1) was the result of incompatible displacements between the tower walls $(\Delta_r \neq 1)$ at the level immediately above the TFL (refer Fig. 2(b)). These displacement incompatibilities are the direct result of the out-of-plane deformation of the transfer plate as shown in Fig. 2(f).

Strutting forces that are developed in the connecting elements in between adjacent tower walls is shown in Fig. 2(c). Interestingly, the amount of increase in the shear force demand as described diminishes rapidly up the height of the building and is negligible at only two-to-three storeys above the TFL (refer Fig. 2(d)).

3. In-plane strains between tower walls above TFL

Strutting forces occurring in between adjacent tower walls can be resulted from differential wall

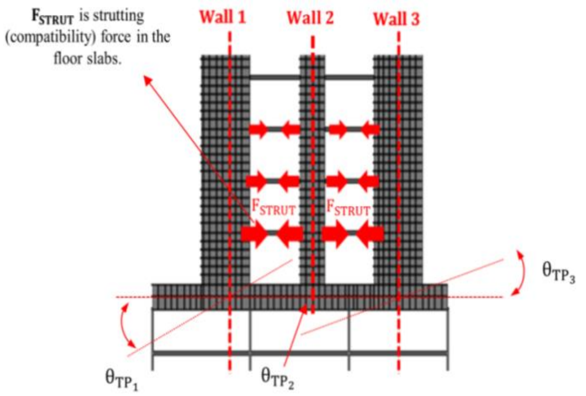

Fig. 3 Introducing F_{STRUT}, ε_{STRUT} and $\Delta\theta_{TP}$

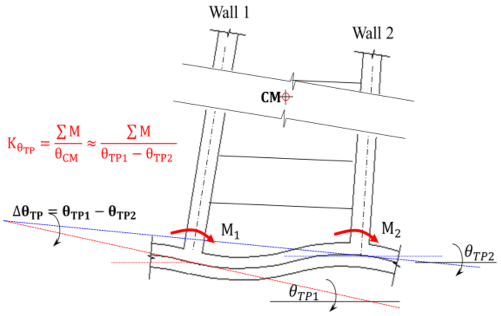

Fig. 4 Angle of rotation at base of tower walls

deflections together with in-plane compatibility restoring actions of the connecting slabs (Fig. 3). The magnitude of the strutting force developed in a connecting member (e.g. link beam and slab) is the product of the in-plane strains that are associated with the differential deflection of adjacent tower walls and the axial stiffness of the member. Thus, the expression to solve for the strutting force (F_{STRUT}) is shown by Eq. (1)

$$F_{STRUT} = \varepsilon_{STRUT} \times E_C A_{eff} \tag{1}$$

where ε_{STRUT} is the in-plane strain in between two adjacent tower walls above the TFL and effective slab area (A_{eff}) is the product of the width of the column-strip and the gross thickness of the slab. The amount of in-plane strain (ε_{STRUT}) is in turn dependent on differences in the angle of rotation of two adjacent tower walls at their base. Parameter $\Delta\theta_{TP}$ (which is θ_{TP1}-θ_{TP2} or θ_{TP2}-θ_{TP3}) is introduced herein as the parameter characterising the differential wall rotation (refer Fig. 4). Should wall nos. 1 and 3 have identical dimension then the value of θ_{TP1}-θ_{TP2} and θ_{TP2}-θ_{TP3} are dependent on the positioning of the wall along the supporting span. Direct correlation between ε_{STRUT} and $\Delta\theta_{TP}$ as modelling parameters is confirmed by the comparison of the ε_{STRUT} profiles for varying values of $\Delta\theta_{TP}$ (Fig. 5). This correlation has also been confirmed for a building which is subjected to simulated earthquake ground accelerations. The time histories of the F_{STRUT} (hence ε_{strut}) and $\Delta\theta_{TP}$ obtained from the analysis (also performed on ETABS) of record no. 3 (Table A-1) are plotted in Fig. 6 on the same graph. Clearly the two quantities are directly correlated.

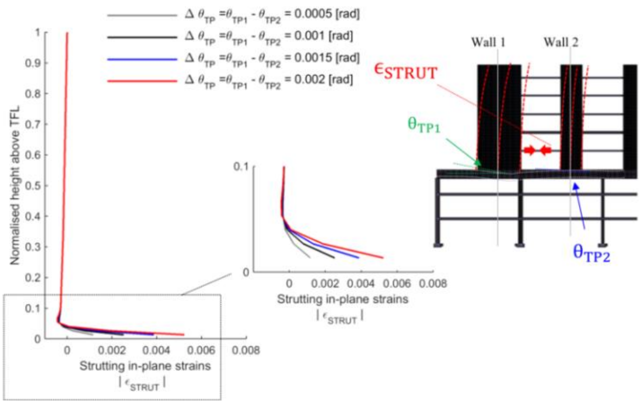

Fig. 5 In-plane strains between walls and differential angle of rotation at their base $\Delta\theta_{TP} = \theta_{TP1}$- θ_{TP2}

4. Analytical modelling of the flexibility index

In section 3, the strutting force of a link element connecting two adjacent tower walls has been shown to be correlated with the value of $\Delta\theta_{TP}$. To further illustrate these dependencies, more linear time history analyses have been performed on several building models with different transfer plate rigidities (thicknesses). The parameter α_r is introduced as a measure to quantify the relative flexural stiffness of the transfer plate $(E_cI)_{TP}$ to that of the tower wall $(E_cI)_{wall}$ (Eq. (2)). For each simulation, the maximum strutting strains in the floor slabs (ε_{STRUT}) are plotted (in Fig. 7) against corresponding values of $\Delta\theta_{TP}$ at the base of walls 1 & 3. The correlation (ε_{STRUT}-$\Delta\theta_{TP}$) is consistently linear as shown in Figs. 7(a)-(f). The slope of the correlation is defined herein as the *Flexibility Index* (*FI*). Importantly, this slope (or value of *FI*) is shown to be dependent on the value of α_r. Thus, the in-plane strain (ε_{STRUT}) may be expressed as the product of *FI* and $\Delta\theta_{TP}$ as shown by Eq. (3).

$$\alpha_r = \sqrt{\frac{(E_C I)_{TP}}{(E_C I)_{wall}}} \tag{2}$$

$$\varepsilon_{STRUT} = FI \times \Delta\theta_{TP} \tag{3}$$

The combined effects of $\Delta\theta_{TP}$ and α_r on the magnitude of the strutting forces F_{STRUT} between two adjacent tower walls are well demonstrated in Fig. 7. It is shown further in Fig. 8 that higher values of FI (meaning higher strutting forces) can be developed in between very stiff tower walls in which case the value of α_r is less than 0.4. On the other hand the magnitude of the strutting forces can be reduced by as much as 60% with relatively flexible tower walls in which case the value of α_r is greater than one.

In cases with multiple tower walls above the TFL α_r is calculated based on the sectional properties of the most flexible wall in the assembly (maximum of three walls for interior bays and two walls for the exterior bays). Where a stiff continuous core shaft is present, α_r is calculated based on the properties of the transferred tower wall connected to the core (verifications are presented in Section 6).

In the most conventional building set-out, the tower

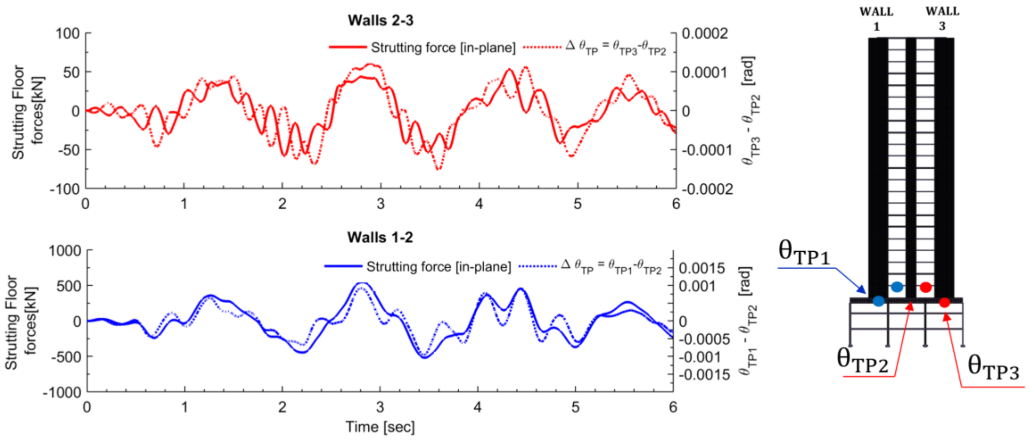

Fig. 6 Time-histories of In-plane strutting forces between walls and differential angle of rotation at their base $\Delta\theta_{TP} = \theta_{TP1}$-$\theta_{TP2}$

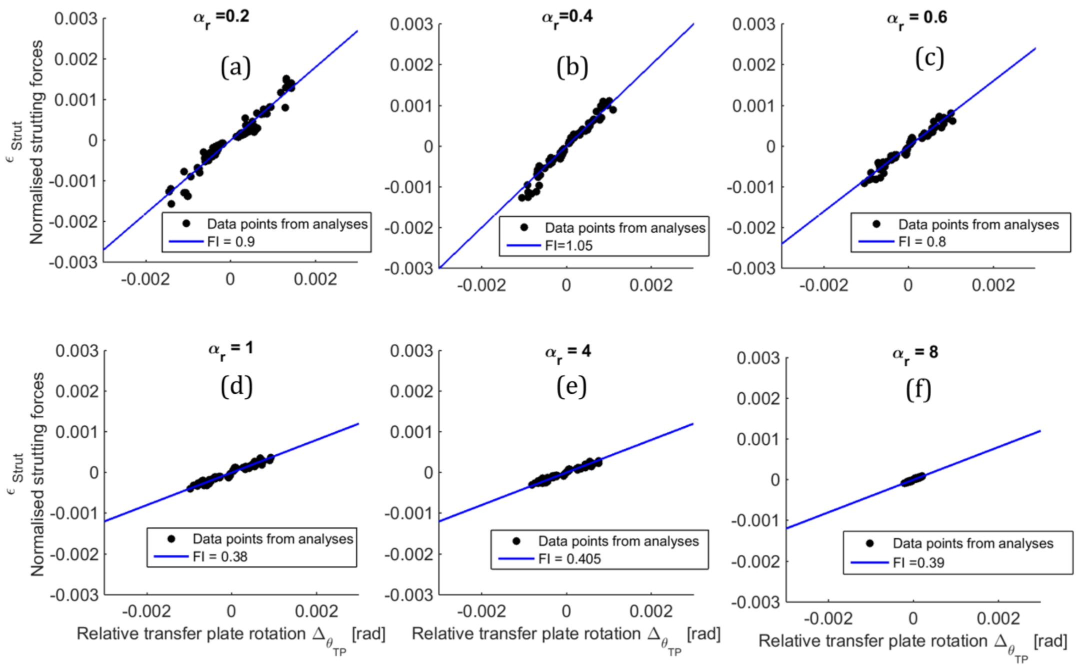

Fig. 7 Effects of α_r on strutting forces in between tower walls (record nos. 3-9)

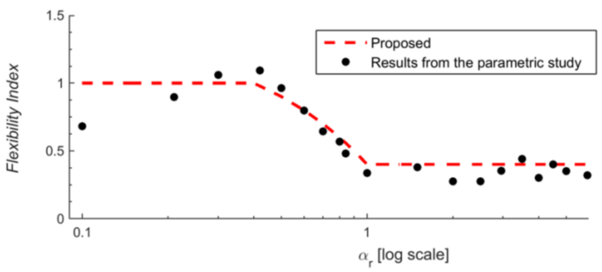

Fig. 8 Correlation of Flexibility Index with α_r

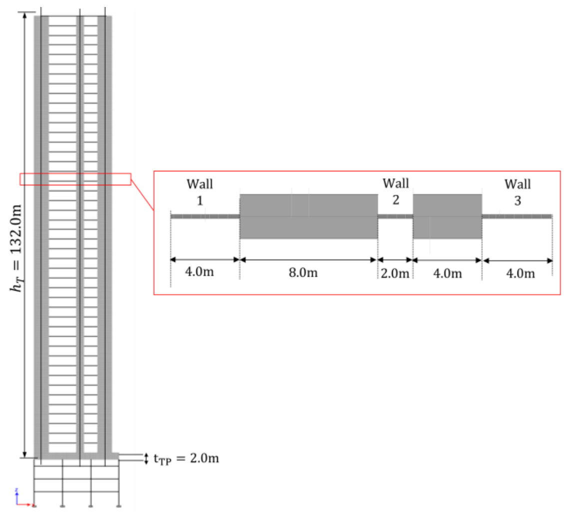

Fig. 9 2D model of a building with tower walls spaced at different intervals

structure caters residential apartments or office spaces that are supported by transferred structural walls typically spaced at 4 m-8 m intervals. Accordingly, the in-plane stiffness of the connecting slabs (defined as $E_c\, A_{eff}/L_{slab}$) varies across the different walls in a storey depending on the span length of the slab (L_{slab}). Intuitively this variation (in-plane stiffness) entails that the strutting forces

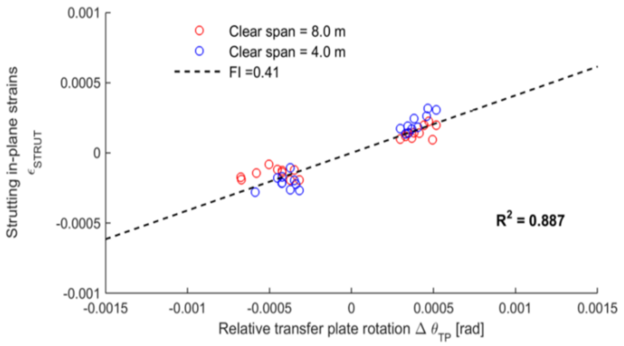

Fig. 10 Peak strutting strains vs. $\Delta\theta_{TP}$ for the case study building

Table 1 Sectional properties of the walls

Wall 1	6000×600	$\alpha_r = 0.3$
Wall 2†	6000×300	$\alpha_r = 0.6$
Wall 3†	3600×300	$\alpha_r = 2.2$
Wall 4†	1500×300	$\alpha_r = 2.2$
Wall 5	1900×150	

† Wall sectional properties used for calculating the value of α_r

in the slabs vary depending on their aspect ratio (slenderness). However, the extent of the in-plane slab strains (ε_{STRUT}) has been found to be independent of the length of the slab's clear span. This is clearly illustrated when plotting the peaks of ε_{STRUT} along with the corresponding values of $\Delta\theta_{TP}$ between walls 1|2 and 2|3 in the 2D case study building shown in Fig. 9. The 2D model of the building is similar to the building model examined earlier with the exception of the unequal span lengths between the transferred walls.

It is illustrated in Figs. 10-11 that larger in-plane deformations (δ_{slab}) are imposed on the longer slab by the tower walls in order that the magnitude of ε_{STRUT} remains literally unchanged for a given value of $\Delta\theta_{TP}$ and α_r as inferred from Eq. (4).

$$\varepsilon_{\mathrm{STRUT}} = \frac{\delta_{slab}}{\mathrm{L_{slab}}} = \frac{\mathrm{F_{STRUT}}}{\mathrm{E_C A_{eff}}} \quad (4)$$

In summary the value of F_{STRUT} can be estimated using Eq. (5) which was derived by combining Eqs. (1)-(2).

$$F_{STRUT} = FI \times \Delta\theta_{TP} \times E_c A_{eff} \quad (5)$$

The robustness of the flexibility index which is defined diagrammatically in Fig. 8 is next examined for a tower structure comprising multiple connected structural walls. The building model shown in Fig. 12 is employed in linear time history analyses using records no.1-4 (see Table A-1 in Appendix A).

The values of parameter α_r for successive walls have been computed based on the sectional properties of the flexible wall in the assembly and were found to be 0.3, 0.6, 2.2 and 2.2 for slabs connecting walls 1|2, 2|3, 3|4 and 4|5 respectively (dimensions of the tower walls are summarised in Table 1).

It is shown in Fig. 13 that larger compatibility forces (in the connecting slabs) are required to restore displacement

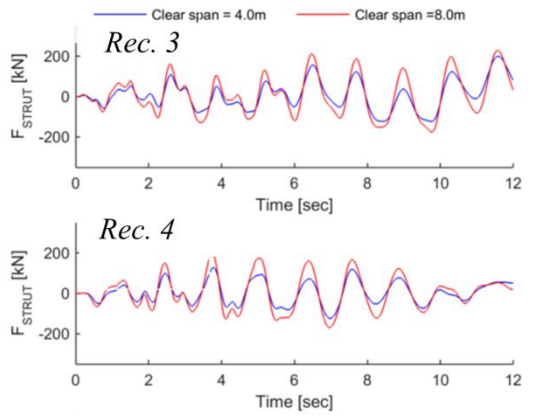

(a) F_{STRUT}

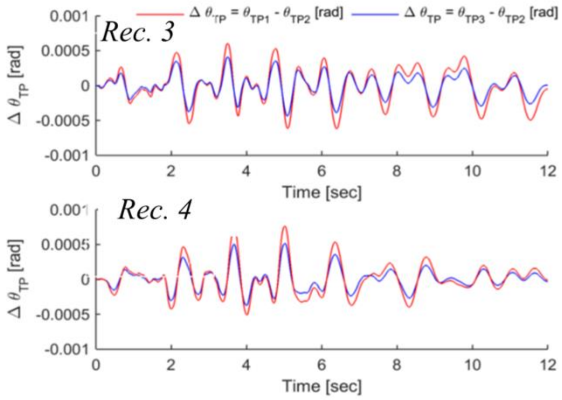

(b) $\Delta\theta_{TP}$

Fig. 11 Sample time history results for (a) F_{STRUT} and (b) $\Delta\theta_{TP}$ (rec Nos. 3-4)

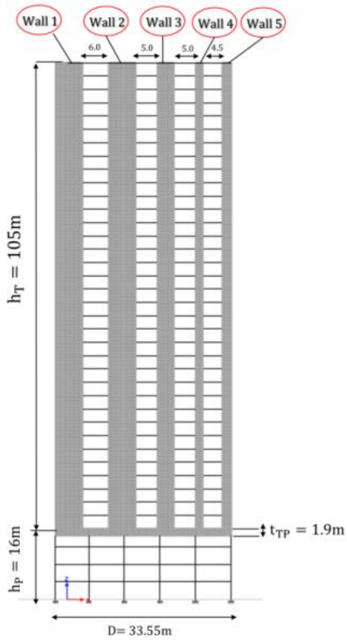

Fig. 12 Model of a building with multiple tower walls with different stiffness

incompatibilities between the stiffer walls (i.e., walls 1|2) compared with the in-plane force demands in the floor slab connecting walls 3|4 (440 kN and 220 kN respectively). The

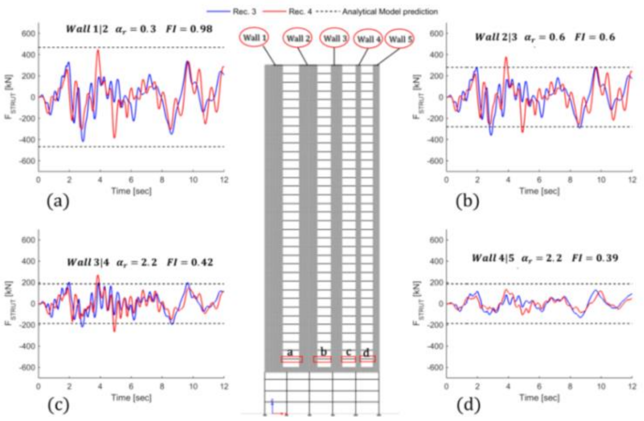

Fig. 13 Strutting (compatibility) force demands in the floor slabs

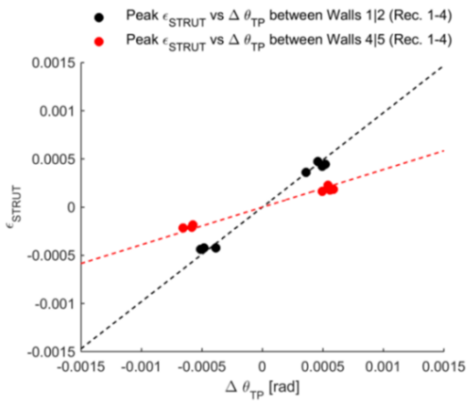

(a) Sample results (peaks)

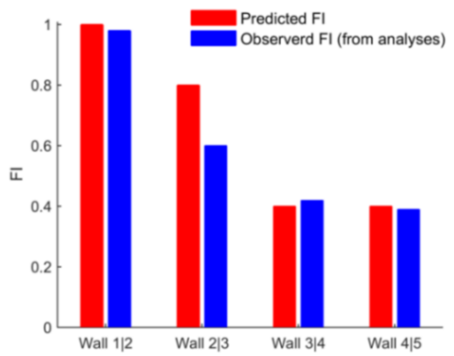

(b) Comparison of predicted and observed FI values

Fig. 14 Flexibility index values for the different tower walls

proposed analytical model is therefore well capable of capturing the interdependency between the strutting force (and strain) as a function of the relative stiffness of the connected walls (as characterised by parameter α_r). This is achieved by the use of the flexibility index (shown in Fig. 8) where higher values of FI are assigned to the stiffer tower walls (see Fig. 14 (a)-(b)).

5. Analytical modelling of peak rotational demand on the building

It was demonstrated in Sections 3 & 4 that the strutting forces that are developed in between adjacent tower walls depend on the value of $\Delta\theta_{TP}$ which characterises the differential tower wall deflections. The calculation of the $\Delta\theta_{TP}$ parameter can be computationally intensive. Thus, other displacement related parameters have been explored to obtain approximate estimate for this parameter. In a proposed simplified procedure for use in the design office the value of $\Delta\theta_{TP}$ is approximated by the angle of drift of the building tower at its mid-height level (i.e., at the level of the centre of mass of the tower block). Good consistencies between the two angles of rotation mean that the amount of in-plane stresses, and strains, developed between two adjacent tower walls can be predicted conveniently by referring to the global displacement (and rotational) demand of the tower block as a whole.

The degree of consistencies has been tested by way of a parametric study employing 2D building models of varying heights (see Fig. A-2 of Appendix A). The numerical models of the wall-plate subassemblies have been constructed on program ETABS. The connected tower walls have been subjected to plate rotations at their base and the CM drift of the tower (θ_{CM} at tower's mid-height) has been examined in relation to the differences in transfer plate rotations (i.e., $\Delta\theta_{TP} = \theta_{TP1} - \theta_{TP2}$). The good agreement between the two parameters ($\Delta\theta_{TP}$ and mid-height drift of the tower) is well demonstrated in Fig. 15(a) (for two tower heights: 75 m and 225 m). The vertical line showing the angle of differential rotation between two adjacent tower walls at their bases is superimposed onto a graph showing the variable angle of drift at the centre line of the building up its height. The resulting storey displacement profiles show straight lines (i.e. constant drift) with the value of the slope approximately equal to the value of $\Delta\theta_{TP}$ at the base (refer Fig. 15(b)).

Eq. (5) for estimating the value of F_{STRUT} may therefore be written as follows

$$F_{STRUT} = FI \times \theta_{CM} \times E_C A_{eff} \tag{6}$$

The innovative idea of linking in-plane strains between adjacent tower walls to the (global) angle of drift of the tower wall as a whole (e.g., θ_{CM}) is motivated by the development of a simplified hand calculation procedure which enables strutting forces in the link elements to be predicted with good confidence (provided that the structural configuration and gross dimensions of the tower walls and that of the podium are known, and the stiffness properties of the transfer plate and that of the tower walls are also known). Estimates of the strutting forces can therefore be made without the need to execute memory intensive finite element analysis of the complete model of the tower-podium assemblage.

The simplified calculation model to be presented herein is based on simplifying the tower walls collectively as a rectangular "rigid-body" which is supported on the podium structure (Fig. 16). The elastic stiffness of the rotational spring (also positioned at the base of the rectangular rigid body) is to emulate effects of the shortening-lengthening (push-pull) actions of the columns in support of the podium and the building tower above it (Fig. 17(c)). The rotational spring is also to incorporate the effects of the transfer

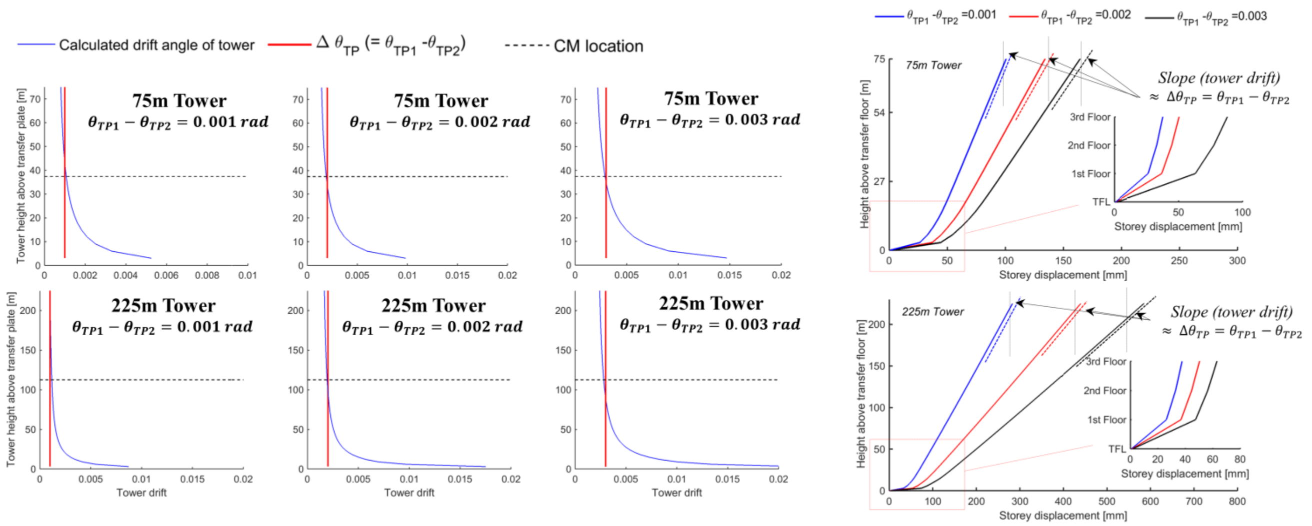

(a) Angle of drift at position of CM in comparison with differential angle of rotation at base of wall $\Delta\theta_{TP} = \theta_{TP1} - \theta_{TP2}$

(b) Tower displacement profiles

Fig. 15 Displacement of tower walls imposed by flexibility at their bases

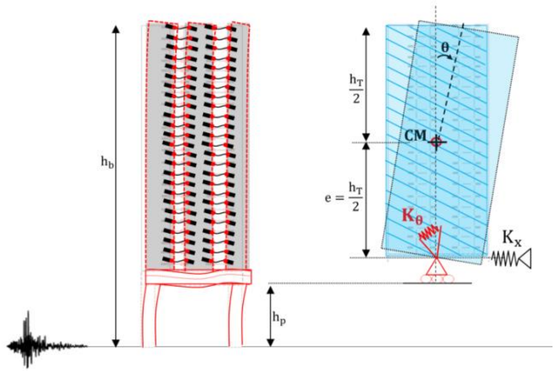

Fig. 16 Schematic representation of the rigid body rotation model

girder's flexibility on the rotations evaluated at the centre of mass (θ_{CM}) of the rigid block (Fig. 16). The sway deflection of the tower as described is actually contradictory to the rigid-body assumption of the simplified model which is, strictly speaking, not representing real behaviour. Thus, results so derived from the simplified calculation method (assuming rigid-body behaviour of the tower block of Fig. 16) need to be verified to demonstrate that errors incurred by the idealisation are within acceptable limits in the practical context (as demonstrated by results presented later in this section and in Section 6).

The value of the elastic stiffness of the translational, and rotational, spring of the rigid-body model (of Fig. 10) is defined by Eqs. (7) and (8) respectively.

$$K_x = \left(\frac{1}{K_T} + \frac{1}{K_P}\right)^{-1} \tag{7}$$

where K_T and K_P are lateral stiffness values for tower and podium structure respectively.

$$K_\theta = \frac{1}{\frac{1}{K_{\theta TP}} + \frac{1}{K_{\theta,podium}}} \tag{8}$$

where meaning of $K_{\theta,podium}$ is as indicated schematically in Fig. 17(c); $K_{\theta_{TP}}$ is the rotational stiffness parameter which is defined as the aggregated bending moment at the base of all the walls ($\sum M$) divided by the rotation at the CM of the tower structure θ_{CM} (Fig. 4). The value of $K_{\theta_{TP}}$ can be estimated using Eq. (9).

$$K_{\theta_{TP}} = E_C t_{TP}^2 W \sqrt{(D/h_T)^3} \tag{9}$$

where D is gross dimension of the building tower (as a whole) in the direction of loading, t_{TP} and W is the thickness and width of the transfer plate, and E_C is the modulus of elasticity of the concrete which the transfer plate is built of.

Eq. (9) has been derived empirically based on results obtained from an extended sensitivity study on the wall-plate assemblages similar to those discussed earlier (see Fig. A-2). The connected tower walls have been subjected to rotations at their base and the CM drift of the tower (θ_{CM} at tower's mid-height) has been examined in relation to the differences in transfer plate rotations (i.e., $\Delta\theta_{TP} = \theta_{TP1} - \theta_{TP2}$). The net overturning moment at the base of the walls ($\sum M$) is evaluated for different scenarios and the rotational stiffness $\left(K_{\theta_{TP}}\right)$ has been computed as $\sum M / \theta_{CM}$. It is worth noting that the $K_{\theta_{TP}}$ parameter is not just representing the flexural stiffness of the transfer plate on its own as it is also representing the degree of restraint on the rotation of the building tower at the centre of mass. Thus, the aspect ratio of the building tower: D/h_T is a parameter in Eq. (9) for estimating the value of $K_{\theta_{TP}}$. Values of $K_{\theta_{TP}}$ so obtained from the analyses have been found to be equal to unity when normalised with respect to the product of the square of the transfer plate thickness (t_{TP}^2), the width of the transfer plate (W), elastic modulus of concrete (E_C) and $\left(\frac{D}{h_T}\right)^{1.5}$ as shown in Figs. 18(a)-(b). Eq. (9) has therefore been verified.

The good agreement between the analytical results and results obtained from the empirical expression (Eq. (9))

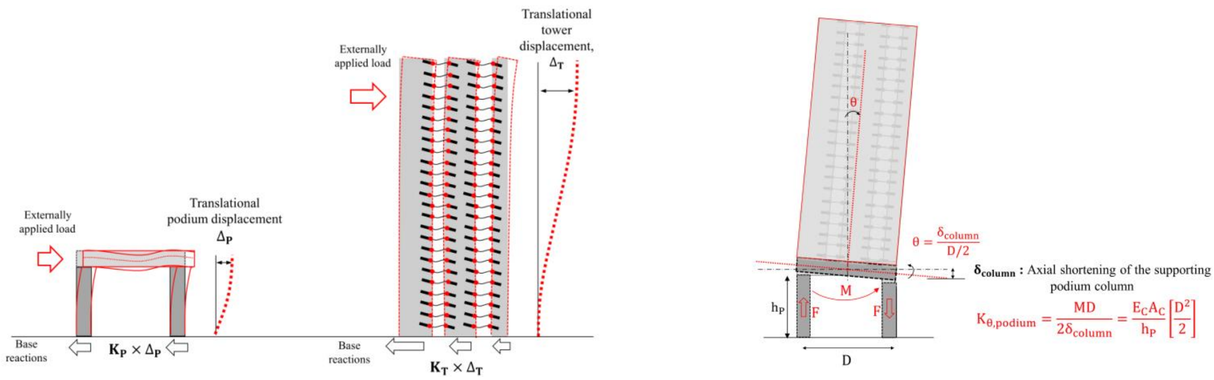

(a) (b) (c)

Fig. 17 Translational and rotational stiffness

contributes to validating the model for predicting the intricate interferences of the transfer plate on the response behaviour of the tower walls of the building. Further validations on a 3D case study building are presented in Section 6 of this paper.

In summary, the spring-connected rigid-body ("rocking") model of the building as depicted in Fig. 16 is complete when the value of K_x and K_θ have been determined using Eq. (7)-(9) and distribution of mass up the height of the tower block is also known. The original computer model of the building may have thousands degrees-of-freedom (DOFs). The use of the rocking model has the number of DOFs reduced to just two: a translational and a rotational DOF. The problem is essentially one of dynamic rotational coupling. A similar approach of modelling has been adopted for analysing dynamic coupling of torsionally unbalanced buildings featuring plan irregularities. The building models employed in those studies have also been reduced to 2 DOFs (Lam *et al.* 2016).

The dynamic rotational coupling analysis of the rigid-body model of the building towers (of Fig. 16) provides predictions for the value of the *Peak Rotational Demand* (PRD) of the building as a whole which is defined herein as the maximum rotations experienced at the CM of the tower imposed primarily by the local distortions of the transfer plate. The analytical details of the rotational coupling problem are next examined.

The dynamic equilibrium equations (Eqs. (10)-(11)) are employed to solve for the coupled dynamic properties of the building and the displacement/rotation response behaviour of the tower when subjected to earthquake ground accelerations.

$$m\ddot{x} + K_x(x + e\theta) = 0 \tag{10}$$

$$J\ddot{\theta} + K_x(x + e\theta)\theta + K_\theta\theta = 0 \tag{11}$$

m in Eq. (11) represents the translational mass of the building, *J* (in Eq. (11)) is the mass moment of inertia of the tower, K_θ is the total rotational stiffness of the tower structure above the TFL (defined in Eq. (8)) and K_x is the equivalent translational stiffness of the building (Eq. (7)).

Eqs. (10)-(11) are next normalised with respect to *mr* and mr^2 respectively. The parameter *r* is the radius of gyration of the tower block undergoing rigid body rotations $\left(r = \sqrt{\frac{h_T^2 + D}{12}}\right)$ and b^2 is the ratio of the total rotational and translational stiffness $\left(b^2 = \frac{K_\theta}{K_x}\right)$. In Eq. (13) the normalised equations of dynamic equilibrium are presented in the matrix format. The "eccentricity" *e* defining the rigid body rotation of the tower block is representing the distance between the TFL and the CM of the tower (assumed at mid-height of the tower) as shown in Fig. 16.

$$\begin{bmatrix} 1 & 0 \\ 0 & 1 \end{bmatrix}\begin{pmatrix} \ddot{x}_r \\ \ddot{\theta} \end{pmatrix} + \omega_x^2 \begin{bmatrix} 1 & e_r \\ e_r & (b_r^2 + e_r^2) \end{bmatrix}\begin{pmatrix} x_r \\ \theta \end{pmatrix} = \begin{pmatrix} 0 \\ 0 \end{pmatrix} \tag{12}$$

where $x_r = \frac{x}{r}$; $e_r = \frac{e}{r}$ $\ddot{x}_r = \frac{\ddot{x}}{r}$, $\omega_x^2 = \frac{K_x}{m}$ and

$$b_r^2 = \frac{K_\theta}{K_x}\left(\frac{12}{h_T^2 + D^2}\right) \tag{13}$$

The coupled Eigen solution for conditions of free vibration is obtained for the coupled dynamic properties of the building. Parameters Ω_i and λ_i are introduced as the coupled angular velocity and the angular frequency ratio for the i-th mode of vibration respectively (as shown by Eq. (14)).

$$\Omega_i = \lambda_i\,\omega_x \tag{14}$$

where ω_x is the translational angular velocity of the building. Full details of the derivations have been presented elsewhere (Lam *et al.* 2016, Lumantarna *et al.* 2013). The two coupled angular frequency ratios λ_i are obtained by solving the 2x2 matrix expressed in Eq. (15).

$$\lambda_i^2 = \left(\frac{1 + (b_r^2 + e_r^2)}{2}\right) \mp \sqrt{\left[\frac{1 - (b_r^2 + e_r^2)}{2}\right]^2 + e_r^2} \tag{15}$$

The introduced analytical model prompts a framework for estimating the rotation of the tower at the CM $(\theta_{CM}(t))$ which is primarily imposed by the distortions of the transfer plate as shown by Eq. (16).

$$\theta_{CM}(t) = \sum_{i=1}^{i=2}\left(\frac{\theta_j}{1 + \theta_j^2}\right)\frac{u_{\Omega_i,\zeta}(t)}{r} \tag{16}$$

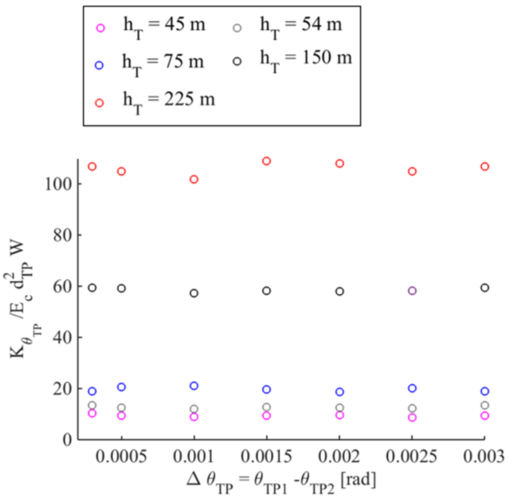

(a) Sample results of $k_{\theta_{TP}}/E_c\, t_{TP}^2 W$

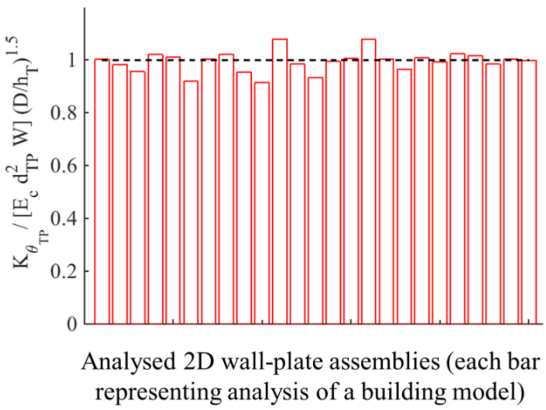

(b) Correlation between analytical $k_{\theta_{TP}}$ and the empirical formulation (Eq. (9))

Fig. 18 Results from the parametric study for determining the parameter $k_{\theta_{TP}}$

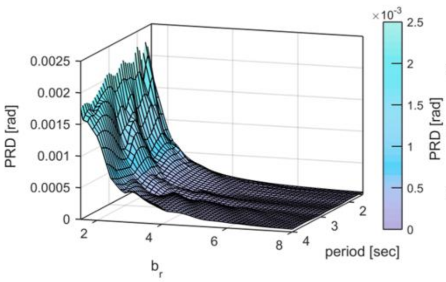

(a) Record Nos. 3-9 ($RSD_{\max} = 107$ mm)

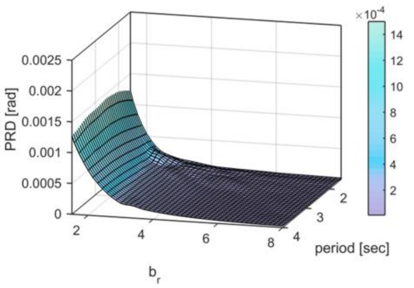

(b) Record Nos. 10-16 ($RSD_{\max} = 67$ mm)

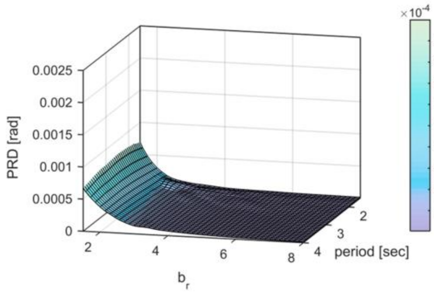

(c) Record Nos. 17-23 ($RSD_{\max} = 38$ mm)

Fig. 19 Effects of (b_r) and $(RSD_{\max})$ on the Peak Rotational Demand (PRD)

where

$$\theta_j = \frac{\lambda_i^2 - 1}{e_r} \tag{17}$$

$u_{\Omega_i,\zeta}(t)$ in Eq. (16) is the damped single-degree of freedom displacement response of an equivalent system with an angular velocity of Ω_i.

The peak rotation demand (PRD) is defined herein as the maximum value of θ_{CM} so obtained from the dynamic analysis (as shown by Eq. (18)).

$$PRD = \max(\theta_{CM}(t)) \geq \max(\Delta\theta_{TP}) \tag{18}$$

Building models similar to that shown in Fig. 1 were employed in a parametric study to investigate trends of PRD on the building structure for varying intensities of ground shaking. The building models have been proportioned to achieve a range of b_r values varying from 0.1 to 6. For all the models the value of K_θ was approximately equal to the value of $K_{\theta_{TP}}$. This was the case since the amount of deformation that was associated with the flexing of the transfer plate was by far higher than that of the (much more rigid) podium structure in below. Thus, the computed value of b_r (Eq. (13)) is dependent on the flexural rigidity (hence thickness) of the transfer plate. The building models have been analysed using three suites of synthetic ground accelerations matching the Australian Standard code spectrum (AS1170.4 2007). Details of the accelerograms used in this study are summarised in Table A-1 of Appendix A. Results of analyses of buildings with increasing fundamental periods of vibration (T_x) and b_r values are presented in Fig. 19.

The PRD trends shown in Figs. 19-21 suggest that the parameter exhibits displacement-controlled behaviour where the values of PRD are insensitive to the building's period (i.e., constant for a given value of b_r). The value of PRD is also shown to decrease with an increase in the transfer plate rigidity and a decrease in the $RSD_{\max}$ of the ground motion (compare Figs. 19(a)-(c)).

The displacement controlled phenomenon which has been shown to govern the PRD on the building prompted the development of a deterministic solution for predicting the value of the PRD given that the values of $RSD_{\max}$ and b_r are known (Eqs. 19(a)-(b) and Fig. 20(a)).

$$\frac{PRD}{\varphi_{ave}} = -0.2 \times \ln(b_r) + 0.6 \tag{19a}$$

where b_r is a dimensionless parameter representing the stiffness properties of the rotational spring which restrains

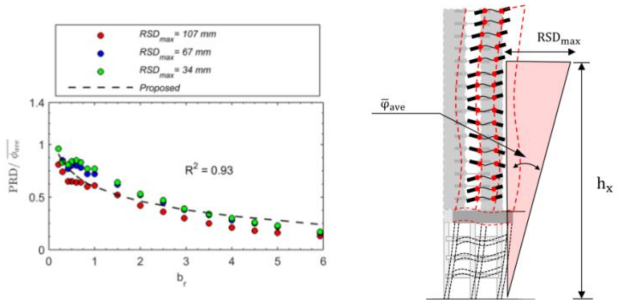

(a) Normalised PRD values obtained from the study (b)Schematic description of the parameter $\overline{\varphi_{\text{ave}}}$

Fig. 20 Analytical model for the estimation of PRD on a building

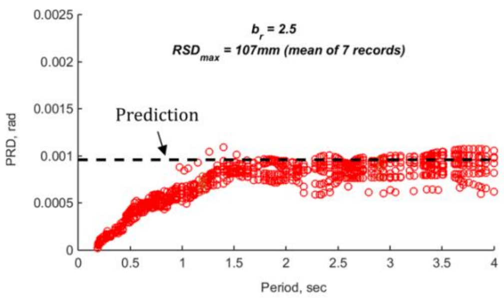

Fig. 21 Results of parametric studies on PRD (b_r=2.5) (based on use of records nos. 3-9 (refer Table A1 of Appendix A)

the rigid-body from rotation (Eq. (13)).

$$\overline{\varphi_{\text{ave}}} = \frac{\text{RSD}_{\text{max}}}{\text{h}_{\text{x}}} \tag{19b}$$

(refer Fig. 20(b) for the diagrammatic illustration)

where h_x is the effective height of the building and may be taken as 0.7 times the total height of the building (h_b); and $RSD_{\max}$ is the highest response spectral displacement value.

It is demonstrated further in Figs. 22-23 that *PRD* as an output parameter from the dynamic rotational coupling analysis (of the simplified rigid-body model of the building) can be used to constrain the values of the differential wall rotation ($\Delta\theta_{TP}$) and in-plane strain (ε_{STRUT}) developed in between adjacent tower walls of the building.

Essentially, *PRD* is used as the parameter to approximate the value of $\Delta\theta_{TP}$ and θ_{CM} in order that Eqs. (5) and (6) can be replaced by Eq. (20) as shown in below.

$$\text{F}_{\text{STRUT}} = \text{FI} \times \text{PRD} \times \text{E}_{\text{C}}\text{A}_{\text{eff}} \tag{20}$$

The simple expression of Eq. (20) for estimating F_{STRUT} provides a conservative estimate for the additional shear forces on the tower walls transferred from the connecting slabs $|\Delta V_{Slab}|$.

A step-by-step flow-chart of the newly developed analytical model for estimating the magnitude of F_{STRUT} is outlined in Fig. 24.

First, the value of PRD is determined based on the translational and rotational stiffness of the building and the value of $RSD_{\max}$ of the design level earthquake (obtained from the design displacement response spectrum). The relative stiffness ratio (α_r) is computed based on the sectional properties of the transferred wall (most flexible wall in an assembly) and the flexural rigidity of the transfer plate. The additional shear force on the wall can then be determined by the use of Eq. (20). The calculated force (F_{STRUT}) will need to be added, arithmetically, to the design shear force of the transferred wall.

Designers are cautioned that these forces (F_{STRUT}) are internal and thus might not have been identified in an analysis of the building should the usual “rigid diaphragm” assumption be adopted. Thus, shear demands on the tower walls might have been misrepresented in certain FE analyses of the building (as discussed in details in another publication by the authors Yacoubian *et al*. (2017a)).

6. Case study of the 3D analysis of a building to illustrate the use of the simplified procedure and to verify its accuracies

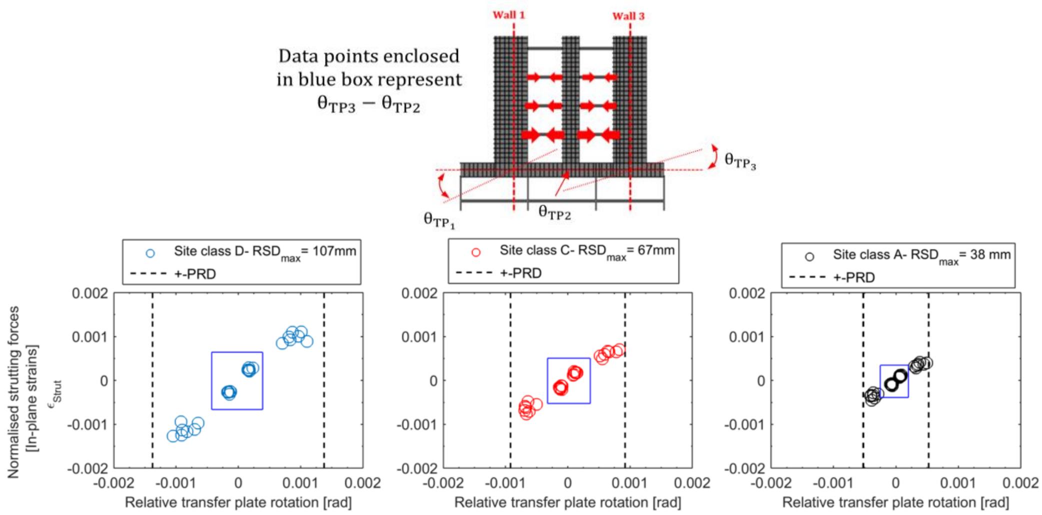

(a) Record Nos. 3-9 (b) Record Nos. 10-16 (c) Record Nos. 17-23

Fig. 22 Peak rotational demand as a parameter to constrain in-plane strutting forces

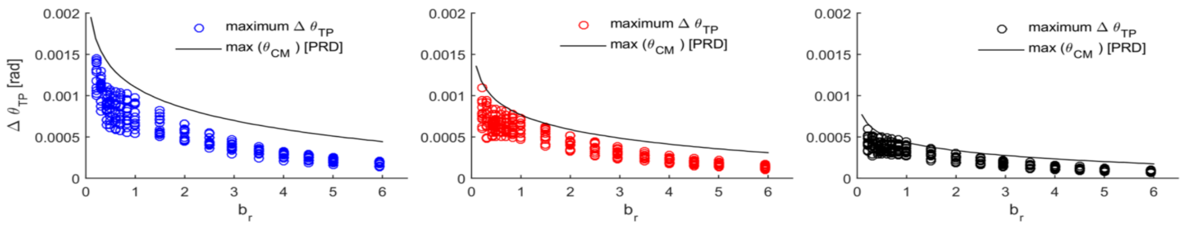

(a) Record Nos. 3-9 ($RSD_{\max}$ = 107 mm)

(b) Record Nos. 10-16 ($RSD_{\max}$ = 67 mm)

(c) Record Nos. 17 – 23 ($RSD_{\max}$ = 38 mm)

Fig. 23 Comparison of $\Delta\theta_{TP}$ and the PRD values obtained from the analyses of the building models

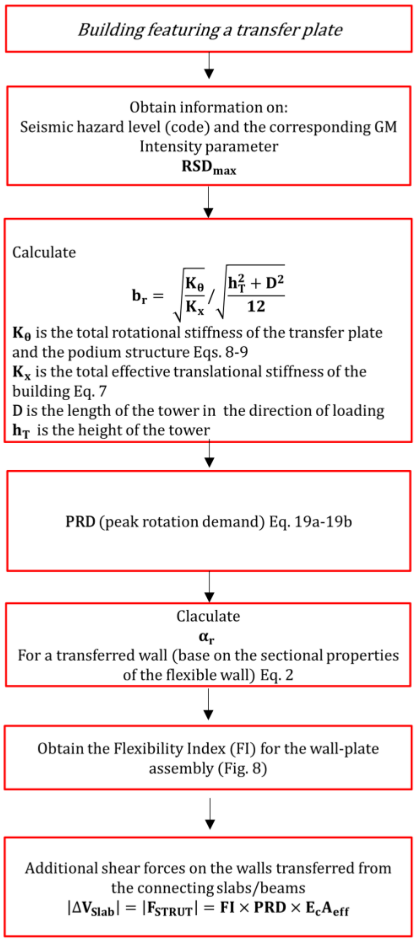

Fig. 24 Design flow chart for calculation of the additional shear force demands on the tower walls above TFL

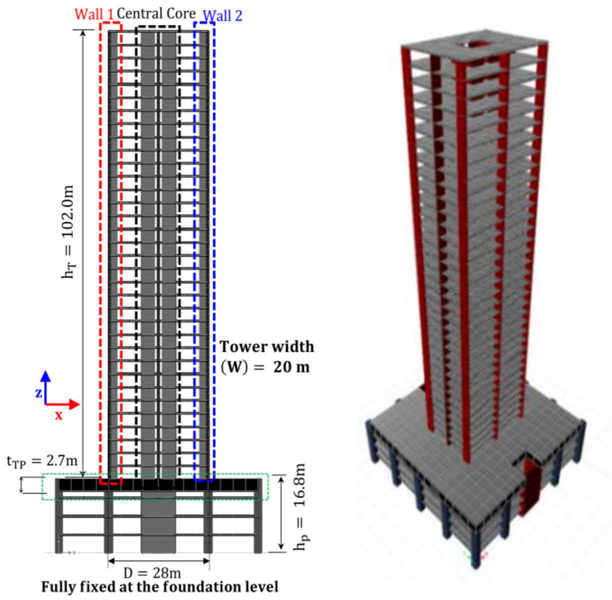

(a) Elevation view of the case study building showing the analysed walls

(b) 3D render of the FE model of the case study building

Fig. 25 Case study building

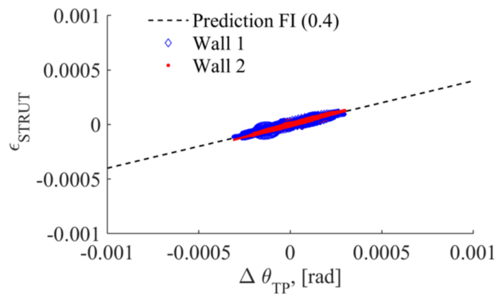

Fig. 26 $\Delta\theta_{TP}$ versus ε_{STRUT} (for records nos. 3- 9)

The case study of the 3D model of a building featuring a transfer structure as shown in Fig. 25 is used to illustrate the application of the simplified analytical procedure introduced in this paper and to verify its accuracies of quantifying the strutting force developed in between adjacent tower walls and the anomalous increase in the shear force demand on tower walls above the TFL. The 120 m reinforced concrete building features a four-storey podium and a 2.7 m thick transfer plate. The 102 m tower structure comprises structural walls and a central core that are coupled by 200mm thick reinforced concrete flat slabs.

The building model has been created in accordance with design guidelines stipulated in Australian Standard (AS 3600, 2009). The lateral load resisting system of the building is designed for wind loads but without taking into account the occurrence of seismic actions.

Floor loads were uniformly applied following Australian Standard recommendations (2002) and are summarised in Table A-3. This coupling analysis provides predictions for the Peak Rotational Demand (*PRD*) which is central to the simplified analytical methodology introduced in this paper. The verification of the accuracies of results from the dynamic coupling analysis is therefore important in terms of verifying the simplified analytical methodology as a whole. A summary of the input parameters and their use in

Table 2 Design details of Wall nos. 1 & 2

Design parameter	Value	Section detail
l_w, **mm**	2000	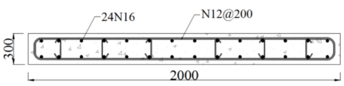
t_w, **mm**	300	
f_c', **MPa**	40.0	
ρ_v, %	0.8	
ρ_t, %	0.38	
Shear capacity $\emptyset V_n$ (AS 3600, 2009),$\boldsymbol{kN}$	862	

calculations as per the simplified calculation procedure are presented in Table A-2 (in Appendix A). In Fig. 27 the roof displacement time histories derived from program ETABS are compared with results of analysis from the 2DOF model to demonstrate consistencies. It is shown further in Fig. 27 that the 2DOF model of the building is capable of accurately estimating the displacement response behaviour of the building. Proportionality between the two parameters: (a) relative transfer plate rotations $\Delta\theta_{TP}$(which is equal

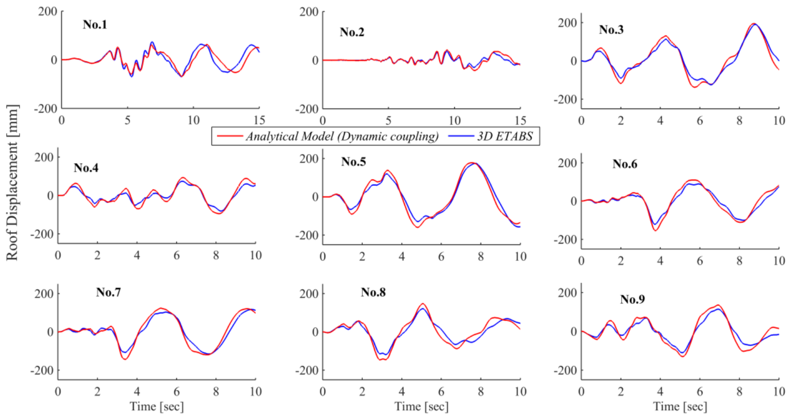

Fig. 27 Comparison of roof displacement time-histories as obtained from the 2DOF model (of Fig. 10) and from the FE Model in ETABS

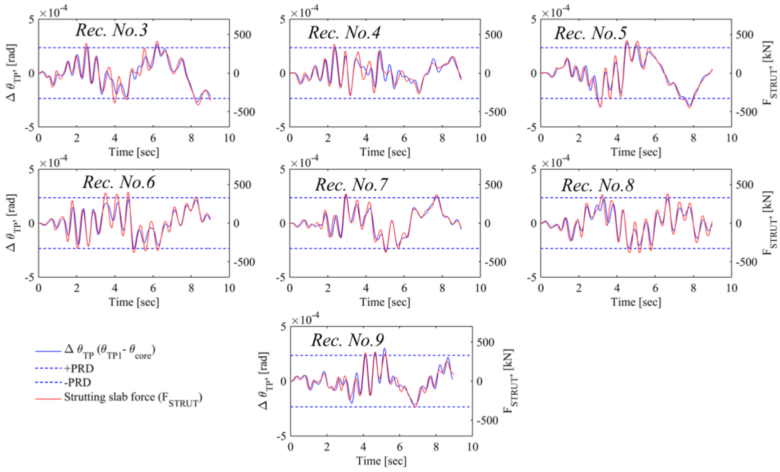

(a) Wall 1

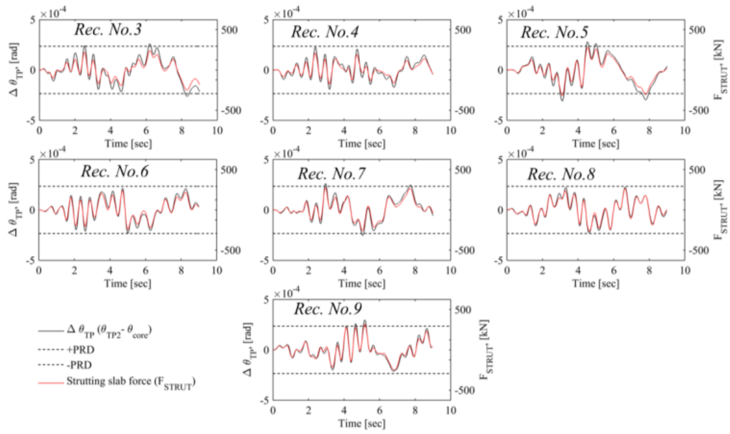

(b) Wall 2

Fig. 28 Slab strutting (in-plane) force and relative base rotation trends for the walls

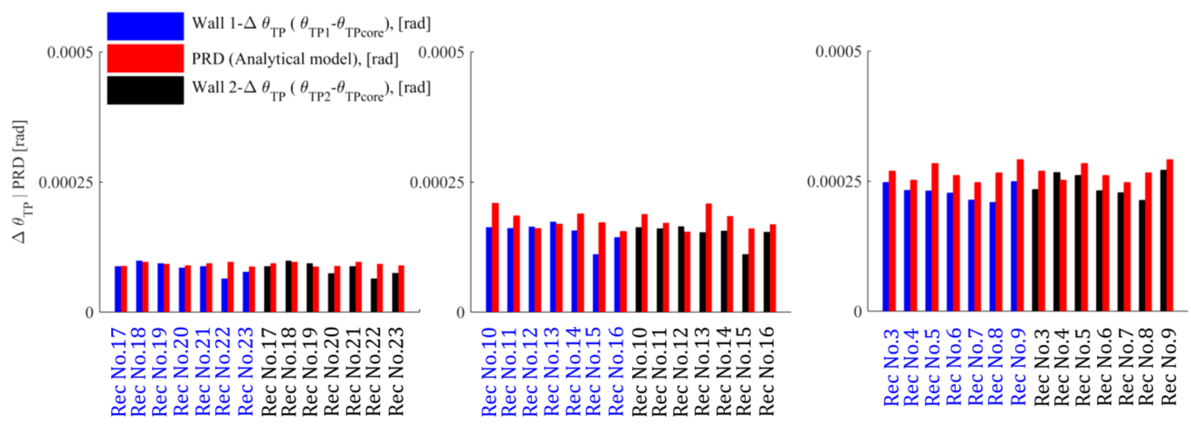

Fig. 29 Comparison between the maximum relative transfer plate rotations (for Walls 1 and 2) with the PRD computed for individual record

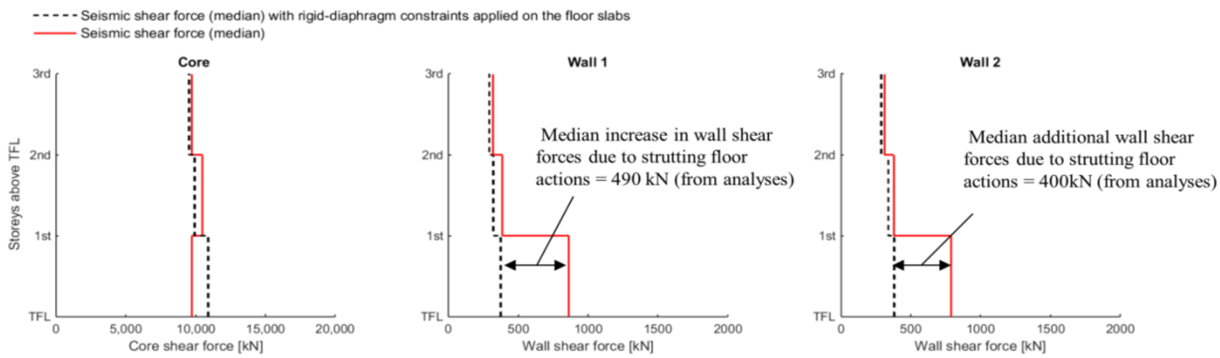

Fig. 30 Shear force distribution above TFL from ETABS (record nos. 3-9)

to $\theta_{TP1} - \theta_{core}, \theta_{TP2} - \theta_{core}$) and (b) strutting forces F_{STRUT} developed in the connecting slabs in between two adjacent tower walls (wall nos. 1 and 2) have been well demonstrated in Figs. 28(a)-(b) in which time-histories of both parameters are superimposed on the same graph.

The flexibility index (FI) for the wall/plate assembly took the value of 0.4 as per recommendations of Fig. 8 (refer also Table A-2 which has every design parameters listed). This value of *FI* which defines the slope of linear correlation between $\Delta\theta_{TP}$ and ε_{STRUT} is consistent with results of FE analysis by program ETABS of the 3D model of the building (noting that Fig. 26 also shows slope of 0.4 in the linear correlation of data retrieved from the FE analysis).

7. Conclusions

Good consistencies between the value of $\Delta\theta_{TP}$ at the base of wall nos. 1 and 2 as derived from FE analyses by program ETABs and the value of PRD (as defined by Eqs. 19(a)-(b)) have also been demonstrated in Fig. 29 in the form of bar charts.

Verification of the FI and PRD parameters are essential as the value of F_{STRUT} is controlled by the two parameters in Eq. (20). The force transfer by the connecting floor slabs in between the tower walls (which has been shown to be the primary contributor to the shear force anomalies in the tower walls) was examined next. Fig. 30 presents the anomalous increase in the shear force demand on the tower wall nos. 1 and 2 at the storey above TFL (the design details of the tower walls 1 and 2 are summarised in Table 2). It is shown that the anomalous increase in the shear force demand on the tower walls above TFL was not revealed by program ETABS when "rigid-diaphragm" assumptions were specified. When the "semi-rigid diaphragm" constraints were applied on the floor slabs the additional shear force demand on the walls was found to be of the order of 500 kN (as shown in Fig. 30 which reports median results from analysis using record nos. 3-9). This prediction from ETABS analysis is also in good agreement with the prediction of 557 kN as per the simplified method introduced in this paper (as listed in Table A-2).

This paper is primarily aimed at addressing the adverse effects of the flexing of the transfer structure on the shear force demand on the tower walls above the TFL. The shear force anomalies have been resulted from significant strutting forces (F_{STRUT}) that are developed in the connecting slabs (or beams) in between adjacent tower walls.

The amount of strutting force (and the in-plane strain: F_{STRUT}) has been shown to be linearly correlated with the differential rotation of adjacent tower walls at their base ($\Delta\theta_{TP}$). The slope of the correlation is the *Flexibility Index* (FI) which is a function of the relative stiffness of the transfer structure and the tower wall. The differential wall rotation is in turn correlated with the angle of drift of the building at mid-height level. A 2DOF model of the building tower has been used to provide predictions for the value of the *Peak Rotational Demand* (PRD) of the building tower as a whole which can be taken as a conservative estimate of the value of $\Delta\theta_{TP}$. The value of F_{STRUT} may then be expressed as the product of FI, PRD and $E_C A_{eff}$ which is the axial stiffness of the connecting element.

The actual modelling of the interference by the transfer structure is highly complex and bears much weight on the rigour employed in the construction of the numerical (FE) model of the building. In the absence of detailed guidelines on modelling such effects, this simple analytical tool (which can be conveniently programmed on a single spreadsheet) is intended to assist the design engineer in quantifying the adverse slab-wall interactions (occurring above the TFL) which are imposed by the transfer structure.

It should be noted that the model assumes linear elastic behaviour of the building components. Thus, the proposed methodology has limitations and need be further developed for use as a seismic safety tool. Nevertheless, this assumption may well be justified for practical purposes in structural design. From a broader perspective, the developed technique sheds light on the appropriateness of the use of displacement-based principles for simplifying highly complex interferences by the transfer structure on the response behaviour of the building.

References

AS 1170.0 (2002), Structural Design Actions-Part 0: General Principals, SAI Global Limited under licence from Standards Australia Limited, Sydney, NSW 2001, Australia.

AS 1170.4. (2007), Structural Design Actions-Part 4: Earthquake Actions in Australia, Sydney, NSW 2001, Australia.

AS 3600 (2009), Concrete Structures, SAI Global Limited, Sydney, NSW 2001, Australia.

ASCE 7-10 (2010), Minimum Design Loads for Buildings and Other Structures, American Society of Civil Engineers.

Chopra, A.K. (1995), *Dynamics of Structures*, Prentice Hall, New Jersey.

European Committee for Standardization (CEN) (2005), Eurocode 8: Design of Structures for Earthquake Resistance-Part 1: General Rules, Seismic Action and Rules for Buildings, European Committee for Standardization (CEN), Brussels, Belgium.

Habibullah, A. (1997), *ETABS-Three Dimensional Analysis of Building Systems*, Users Manual, Computers and Structures Inc., Berkeley, California.

TBI (2010), Guidelines for Performance-based Seismic Design of Tall Buildings, Pacific Earthquake Engineering Research Center.

Kuang, J. and Zhang, Z. (2003), "Analysis and behaviour of transfer plate-shear wall systems in tall buildings", *Struct. Des. Tall Spec. Build.*, **12**, 409-421.

Lam, N., Lumantarna, E. and Wilson, J. (2016), "Simplified elastic design checks for torsionally balanced and unbalanced low-medium rise buildings in lower seismicity regions", *Earthq. Struct.*, **11**(5), 741-777.

Lee, H.S. and Hwang, K.R. (2015), "Torsion design implications from shake-table responses of an RC low-rise building model having irregularities at the ground story", *Earthq. Eng. Struct. Dyn.*, **44**, 907-927.

Li, C., Lam, S., Zhang, M. and Wong, Y. (2006), "Shaking table test of a 1: 20 scale high-rise building with a transfer plate system", *J. Struct. Eng.*, **132**, 1732-1744.

Lumantarna, E., Lam, N. and Wilson, J. (2013), "Displacement-controlled behavior of asymmetrical single-story building models", *J. Earthq. Eng.*, **17**, 902-917.

Lumantarna, E., Lam, N., Wilson, J. and Griffith, M. (2010), "Inelastic displacement demand of strength-degraded structures", *J. Earthq. Eng.*, **14**, 487-511.

Mwafy, A. and Khalifa, S. (2017), "Effect of vertical structural irregularity on seismic design of tall buildings", *Struct. Des. Tall Spec. Build.*, **26**(18). e1399.

PEER (2015), *PEER Strong Motion Data Base*, Pacific Earthquake Engineering Research Center, http://peer.berkeley.edu/smcat/index.htm.

PEER/ATC (2010), Modeling and Acceptance Criteria for Seismic Design and Analysis of Tall Buildings, Redwood City, CA: Applied Technology Council in Cooperation with the Pacific Earthquake Engineering Research Center.

Priestley, J.N., Calvi, G.M. and Kowalsky, M.J. (2007), *Displacement-based Seismic Design of Structures*, IUSS Press.

Priestley, M. (1997), "Displacement-based seismic assessment of reinforced concrete buildings", *J. Earthq. Eng.*, **1**, 157-192.

Qian, C.G. and Wang, W. (2006), "Effect of the thickness of transfer slab on seismic behavior of tall building structure", *Optim. Cap. Constr.*, **27**, 98-100.

Seismosoft. SeismoArtif (Version 5.1.2 Build:1, June 2014). Retrieved from www.seismosoft.com.

Su, R.K.L, Tsang, H. and Lam, N. (2011), "Seismic design of buildings for Hong Kong conditions", Hong Kong Institution of Engineers.

Su, R.K.L (2008), "Seismic behaviour of buildings with transfer structures in low-to-moderate seismicity regions", Department of Civil Engineering, The University of Hong Kong, Hong Kong, China.

Su, R.K.L and Cheng, M. (2009), "Earthquake-induced shear concentration in shear walls above transfer structures", *Struct. Des. Tall Spec. Build.*, **18**, 657-671.

Su, R.K.L., Chandler, A.M., Li, J.H. and Lam, N. (2002), "Seismic assessment of transfer plate high rise buildings", *Struct. Eng. Mech.*, **14**, 287.

Tang, T.O. and Su, R.K.L. (2015), "Gravity-induced shear force in reinforced concrete walls above transfer structures", *Proc. Inst. Civil Eng., Struct. Build.*, **18**(6), 657-671.

Tsang, H.H., Su, R.K.L, Lam, N. and Lo, S. (2009), "Rapid assessment of seismic demand in existing building structures", *Struct. Des. Tall Spec. Build.*, **18**, 427-439.

Yacoubian, M., Lam, N., Lumantarna, E. and Wilson, J.L. (2017a), "Effects of podium interference on shear force distributions in tower walls supporting tall buildings", *Eng. Struct.*, **148**, 639-659.

Yacoubian, M., Lam, N., Lumantarna, E. and Wilson, J.L. (2017b), "Simplified design checks for buildings featuring transfer structures in regions of lower seismicity", *The 2017 World Congress on Advances in Structural Engineering and Mechanics (ASEM17)*, Ilsan (Seoul), Korea.

Zhitao, Z.J.W.G.L. (2000), "Dynamic properties and response of the thick slab of transfer plate models with dual rectangular shape in tall building", *Build. Struct.*, **6**, 010.

Appendix A

Table A-1 Description of the accelerograms used in the study

Record Reference	Earthquake name	Source
No. 1	Friuli (1976)	PEER(PEER, 2015)
No. 2	Northridge (1994)	PEER(PEER, 2015)
No.3-9	D-x	Code compliant suite of records for Site class D (AS1170.4, 2007) SeismoArtif (SeismoSoft)
No.10-16	C-x	Code compliant suite of records for Site class C (AS1170.4, 2007) SeismoArtif (SeismoSoft)
No.17-23	A-x	Code compliant suite of records for Site class A (AS1170.4, 2007) SeismoArtif (SeismoSoft)

Table A-2 Detailed calculation summary for the case study building

$\mathbf{K_T}$, kN/m	Step-by-step calculation procedure summarised in Yacoubian *et al.* 2017b	17841
$\mathbf{K_P}$, kN/m	Step-by-step calculation procedure summarised in Yacoubian *et al.* 2017b	3369410
$\mathbf{K_x}$, kN/m	$(1/17841 + 1/3369410)^{-1}$	17747
$\mathbf{r}$, m	$\sqrt{(102^2 + 28^2)/12}$	30.53
$\mathbf{K_{\theta_{TP}}}$ kNm/rad (Eq. (9))	$31.62 \times 10^6 \times 2.7^2 \times 20 \times (28/102)^{1.5}$	7.41×10^8
$\mathbf{K_\theta}$, kNm/rad (Eq. (8))	For infinitely stiff podium columns and fixed at the base $\mathbf{K_\theta} = \mathbf{K_{\theta_{TP}}}$	7.41×10^8
$\mathbf{b_r}$	$\left[\sqrt{7.41 \times 10^8/17747}\right] / 30.53$	6.69
PRD (Eq. (19a)-(19b)), rad	$(107/99346)[-0.2\ln(6.69) + 0.6]$	0.00024
	$(67/99346)[-0.2\ln(6.69) + 0.6]$	0.00015
	$(38/99346)[-0.2\ln(6.69) + 0.6]$	8.44×10^{-5}
$\boldsymbol{\alpha_r}$ (Eq. (2))	$\sqrt{\left(\frac{1}{12}2.7^3 \times 5.02\right)/\left(\frac{1}{12}2.0^3 \times 0.3\right)}$	6.42
FI, 1/rad	From Fig. 8	0.4
$\mathbf{F_{STRUT}}$, kN Records No: 3-9	$0.4 \times 0.00024 \times 5.88 \times 10^6$	557
$\mathbf{F_{STRUT}}$, kN Records No: 10-16	$0.4 \times 0.00015 \times 5.88 \times 10^6$	349
$\mathbf{F_{STRUT}}$, kN Records No: 17-23	$0.4 \times 8.44 \times 10^{-5} \times 5.88 \times 10^6$	198

Table A-3 Floor load assignment

	Tower	Podium
Additional dead loads, $\boldsymbol{kN/m^2}$	1	1.2
Live loads, $\boldsymbol{kN/m^2}$	2	5

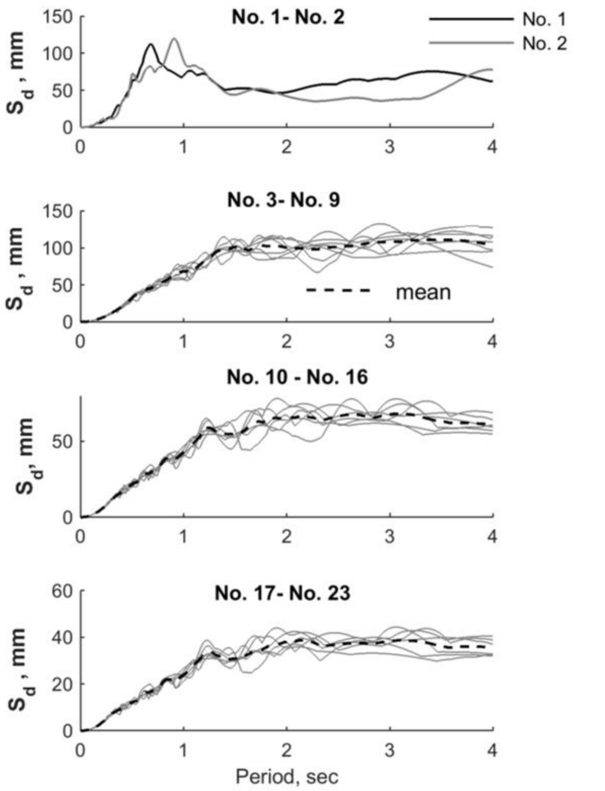

Fig. A-1 Spectral displacements for the records used in the study

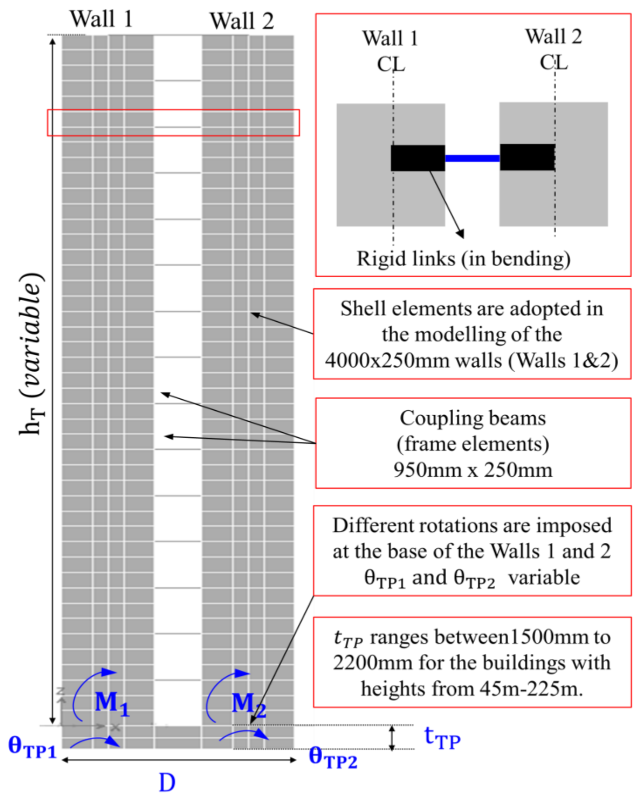

Fig. A-2 2D model used in the parametric study (Section 5) constructed on the program ETABS